Reliability-based topology optimization under shape uncertainty modeled in Eulerian description

Reliability-based topology optimization under shape uncertainty modeled in Eulerian description

Yuki Sato · **Kazuhiro Izui** · **Takayuki Yamada** · **Shinji Nishiwaki** · **Makoto Ito** ·
Nozomu Kogiso

Abstract This paper presents a reliability-based topology optimization method under geometrical uncertainties. First, we briefly introduce the concept of topology optimization. Then, we explain how shape uncertainty is modeled in Eulerian description, using an advection equation and a Karhunen-Loève expansion. Based on the shape uncertainty modeling, we formulate a reliability measure for the shape uncertainty, briefly introducing the inverse reliability method. Two optimization problems, a minimum mean compliance problem and an optimum design problem for a compliant mechanism, are then formulated using the proposed shape uncertainty modeling. The design sensitivity analysis for the reliability analysis and optimization procedure, performed using the adjoint variable method, is then explained. A two-level optimization algorithm is constructed next, in which the inner iteration is used for reliability analysis and the outer is used for updating design variables. Finally, three numerical examples are provided to demonstrate the validity and the utility of the proposed method.

Keywords Topology optimization · Reliability design · Shape uncertainty · Karhunen-Loève expantion · Performance measure approach

Y. Sato · K. Izui · T. Yamada · S. Nishiwaki
Department of Mechanical Engineering and Science, Kyoto University,
Kyotodaigaku-Katsura C3, Nishikyo-ku, Kyoto 615-8540, Japan
Tel.: +81-75-383-3602
Fax: +81-75-383-3601
E-mail: satou.yuuki.87x@kyoto-u.jp

M. Ito · N. Kogiso
Department of Aerospace Engineering, Osaka Prefecture University,
1-1 Gakuen-cho, Naka-ku, Sakai, Osaka, 599-8531 Japan

1 Introduction

Topology optimization is a kind of structural optimization that can derive optimal structures based on mathematical and physical principles. Since the pioneering study by Bendsøe and Kikuchi (1988), topology optimization has successfully been applied to various physics problems, including structural (Ma et al, 1995; Nishiwaki et al, 1998; Bendsøe and Sigmund, 1999), heat transfer (Iga et al, 2009; Yamada et al, 2011), multiphysics (Matsumori et al, 2013; Alexandersen et al, 2014; Furuta et al, 2017), and multimaterial (Yin and Ananthasuresh, 2001; Wang and Wang, 2004; Zuo and Saitou, 2017) problems described in the literature.

The industrial application of topology optimization methodologies has attracted much attention for at least a decade. In a topology optimization, consideration of uncertainties in attributes such as load magnitudes and directions, material properties, and shapes, seeks to take into account particular manufacturing situations or usage environments. Geometrical uncertainties arising from manufacturing errors and operational wear may directly affect the physical performance of various devices. Geometrical uncertainties can cause particularly large effects in micro fabrication processes for micro electro mechanical systems (MEMS), due the small geometrical scale. However, since the physical performance of a device depends on the details of its shape in implicit and highly non-linear ways, design engineers can seldom predict the effects of geometrical variations and therefore must modify a design manually to improve it, a time-consuming process. Thus, there is a great need for structural design methods that efficiently consider geometrical uncertainties during the optimization stage.

Optimizations considering uncertainty are mainly classified into robust optimizations and reliability-based optimizations. In robust approaches, the mean and the variance of the response of a device or system is usually minimized

so that the response becomes less sensitive to the particular uncertainty. Previous research related to robust topology optimization has considered uncertainties in load magnitudes and directions (Kogiso et al, 2008), and the location where a load is applied (Guest and Igusa, 2008). Chen et al (2010) proposed a topology optimization method that takes into account the spatially varying uncertainty in a material property in addition to uncertainty in the direction of an applied load, based on the Karhunen-Loève (K-L) expansion, and this work was extended to topology optimization under geometrical uncertainty as mentioned below.

Robust topology optimization methods under geometrical uncertainty have also been proposed. Sigmund (2009) proposed a robust optimization formulation that considered two uniform geometrical variations, i.e., eroded and dilated, using projections with different thresholds. This method was extended to accommodate non-uniform variations by Schevenels et al (2011), with spatially varying thresholds used in a Heaviside projection and thresholds generated with a Monte Carlo method. Lazarov et al (2012) also proposed a method considering non-uniform variations, in which a K-L expansion was used to represent a random field for a threshold, using a finite number of random variables so that the perturbation with respect to these variables yielded additional linear systems amenable to solution without relying on a Monte Carlo method. In these methods, geometrical variations are represented relatively easily as spatially varying thresholds, with the magnitude of erosion or dilation depending on the length scale and radius of an applied density filter.

On the other hand, Jansen et al (2013) proposed a geometrical uncertainty modeling by shifting the center of the density filter kernel using the random perturbation vector, in which the mean and the standard deviation of the performance and their sensitivities were computed by the Monte Carlo method. This method has an advantage, compared to the above threshold based schemes, of the ability to model relatively large uncertain geometrical variations, owing to the Eulerian description. The research group also proposed a Lagrangian approach for sufficiently small geometrical variations by representing them as shifts of the finite element nodes, incorporating geometric non-linearities in the robust topology optimization (Jansen et al, 2015). This Lagrangian approach makes the analytical derivation of the sensitivities much more complex, so they incorporated a semi-analytical approach in which the derivatives of the finite element matrices are computed using finite differences. In a level set-based approach, Guo et al (2013) proposed a level set-based structural optimization method considering boundary uncertainties by assuming that the boundary perturbations are small enough to allow approximation of the objective function using a first-order Taylor expansion. Chen and Chen (2011) proposed a level set-based robust shape and topology optimization in which geometrical variations were modeled by

advection of the level set function with random normal velocities applied on the boundaries extracted as a zero level set, and the statistical moments of performance were evaluated using a Gauss quadrature formula, with evaluation of the objective function required at each quadrature point. Zhang and Kang (2017) proposed a robust shape and topology optimization with stochastic level set perturbation in which geometrical variations were represented by the finite random perturbation applied to the level set function. This method can consider the geometrical variations that create a new hole. The perturbation approaches in the level set method were also applied with the extended finite element method (X-FEM) (Nouy and Clement, 2010; Lang et al, 2015).

Reliability-based design optimization (RBDO) is another powerful approach for considering uncertainties, and is applied in a topology optimization (Kharmanda et al, 2004) in which external loads and geometric dimensions are considered as random variables. In RBDO, limit state functions describing safe and failure states are introduced and the failure probability calculated with these functions is minimized. There are several methods to evaluate failure probabilities, including Monte Carlo simulation (MCS) (Rashki et al, 2014; Alban et al, 2017), surrogate models (Bichon et al, 2011; Xiao et al, 2018), the first-order reliability method (FORM) (Rackwitz and Flessler, 1978), and the second-order reliability method (SORM) (Kiureghian and Stefano, 1991). A MCS is relatively accurate but computationally expensive; the FORM is the most popular method for estimating failure probability, due to its simplicity and efficiency.

Based on such reliability analyses, RBDO problems are usually formulated as two-level nested optimization problems. The FORM uses the reliability index approach (RIA), in which probabilistic constraints are evaluated at the most probable failure point (MPFP), searched for in the inner loop of the optimization procedure. On the other hand, the performance measure approach (PMA) (Tu et al, 1999) is more stable and efficient than the RIA for evaluating probabilistic constraints (Lee et al, 2002; Youn and Choi, 2004). In the PMA, probabilistic constraints are evaluated at the minimum performance target point (MPTP), searched for in the inner loop of the optimization procedure.

One difficulty with the RBDO approach stems from its inherent double-loop structure that incurs high computational cost. Single-loop approaches offer alternatives, such as the single-loop single-vector (SLSV) method (Chen et al, 1997; Kogiso et al, 2012) in which the probabilistic constraint is replaced by an equivalent deterministic constraint. These methods are very efficient for solving RBDO problems that have linear or moderately non-linear limit state functions. On the other hand, in PMAs, several methods have been proposed to improve the robustness and efficiency of MPTP searches, even for problems that have non-linear performance func-

tions (Meng et al, 2015; Ezzati et al, 2015; Keshtegar and Lee, 2016).

Recently, a reliability-based topology optimization method under geometrical uncertainty has also been proposed (Kang and Liu, 2018). This method was based on the PMA, incorporating the random threshold projection and the polynomial chaos expansion to represent the geometrical variations and then to evaluate the stochastic structural response, and successfully obtained the optimized solutions according to the target reliability settings. However, only relatively small geometrical variations were allowed in this method due to the use of the random threshold projection, as pointed out in (Jansen et al, 2013).

In the present study, we propose a method for reliability-based topology optimization under geometrical uncertainties that employs an inverse reliability method based on a PMA and a two-level nested algorithm in the optimization procedure. The proposed method uses an Eulerian description for geometrical variations that does not require the assumption that shape variations are sufficiently small. Consequently, we model geometrical variations with an advection equation in which the advection velocity is given as a random field and represents the magnitude and direction of the variations. Therefore, the advection equation used in the optimization problems here is applied to geometrical variations in addition to physical equilibrium equations, which now depend on the advection equation because physical equilibrium states for perturbed shapes are the focus. Although this yields a complicated dependency of the objective function on design variables, sensitivities for both MPTP searches and the topology optimization can be derived systematically using the adjoint variable method, owing to the implicit description of the geometrical variations in the advection equation.

The remainder of this paper is organized as follows. First, topology optimization is briefly discussed in Section 2. Next, reliability for shape uncertainty is formulated in Section 3, where the shape uncertainty modeling is also proposed, based on an Eulerian description and K-L expansion, and the inverse reliability method is then discussed. In Section 4, two optimization problems are formulated, a minimum mean compliance problem and an optimum design problem for a compliant mechanism. The numerical implementation is discussed in Section 5 and the proposed method is applied to three numerical examples in Section 6. Finally, in Section 7, we conclude this study.

2 Topology optimization

2.1 Material interpolation for topology optimization

The basic idea of topology optimization is the replacement of a structural optimization problem with a material dis-

tribution problem by introducing a characteristic function, $\chi_\Omega \in L^\infty(D; \{0,1\})$, where L^∞ represents a Lebesgue space defined in a fixed design domain D as

$$\chi_\Omega(\boldsymbol{x}) = \begin{cases} 1 & \text{for } \boldsymbol{x} \in \Omega \\ 0 & \text{for } \boldsymbol{x} \in D \setminus \Omega, \end{cases} \tag{1}$$

where Ω represents the material domain, the complementary $D \setminus \Omega$ represents the void domain, and $\boldsymbol{x}$ represents a coordinate vector. Arbitrary shapes and topologies can be expressed as a material distribution in the fixed design domain using the characteristic function, but since it can be discontinuous at every point, a relaxation or regularization technique is usually required, to deal with the ill-posedness of topology optimization problems. The most popular technique is a so-called density method, based on a convexification method (Section 5.2.5 of (Allaire, 2002)), in which the space $L^\infty(D; \{0,1\})$ is replaced by its convex hull $L^\infty(D; [0,1])$. The Solid Isotropic Material with Penalization (SIMP) scheme (Bendsøe and Sigmund, 1999) is an often-used material interpolation scheme in which a material property such as Young's modulus, E, between material and void domains is interpolated as

$$E(\overline{\gamma}) = E_0 \overline{\gamma}^p, \tag{2}$$

where E_0 is the Young's modulus of the material, $\overline{\gamma}$ is a normalized density that interpolates intermediate material properties, and p is a penalty parameter, usually set to 3.

2.2 Heaviside projection method using a PDE-based filter

In topology optimization, a filtering scheme is often used to prevent overly complex sub-structures from appearing and numerical instabilities from occurring (Sigmund and Petersson, 1998; Bourdin, 2001; Guest et al, 2004). In the present study, we use a Heaviside projection method incorporating a Helmholtz-type of partial differential equation (PDE) filter (Lazarov and Sigmund, 2009; Kawamoto et al, 2011), in which an auxiliary design variable field, $\phi \in L^\infty(D; [-1,1])$, is introduced and a PDE filter is then applied to field ϕ as follows:

$$-R^2 \nabla^2 \varphi + \varphi = \phi. \tag{3}$$

where φ is the filtered variable. Note that in Heaviside projection methods, the design variables are conventionally bounded in [0, 1]. But, the raw design variables have no physical meaning and are only used as intermediate mathematical variables (Sigmund, 2007). In the present study, we set the bound to [-1, 1]. The filtered variable is projected to 0/1 by the zero threshold, using a smoothed Heaviside function as follows:

$$\overline{\gamma} = H_\alpha(\varphi) = \frac{1}{1 + \exp(-\alpha \varphi)}, \tag{4}$$
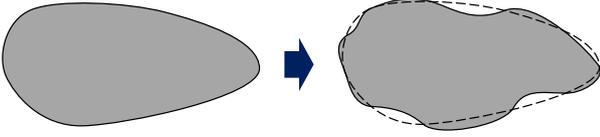
Fig. 1 Schematic of unperturbed and perturbed shapes.

where α is a parameter that controls the curvature of the smoothed Heaviside function. $\overline{\gamma}$ is then used as the normalized density. When $\alpha \to \infty$, the above smoothed Heaviside function corresponds to the Heaviside function.

3 Formulation of reliability for shape uncertainty

3.1 Shape uncertainty modeled in an Eulerian description

To formulate a reliability topology optimization problem considering geometrical uncertainties, they must first be modeled mathematically. Figure 1 is a schematic representation of geometrical variation. Lagrangian and Eulerian descriptions are two possible candidates for modeling such variation. In a Lagrangian description, variations are represented as trajectories of points, such as the nodes of a finite element mesh, and an assumption that variations are sufficiently small is usually required to avoid mesh distortions. On the other hand, in an Eulerian description, the variations are represented by a variation field observed at spatially fixed points. Since a structural configuration is implicitly represented by the characteristic function in a topology optimization, the Eulerian description is especially suitable for modeling geometrical variations, so we use it here. We considered the material derivative of the normalized density in Eulerian description. Shape variations are then formulated with a fictitious advection equation for a normalized density γ with a random velocity $\boldsymbol{V}(\boldsymbol{x})$ as follows:

$$\frac{D\gamma}{Dt} = \frac{\partial \gamma(\boldsymbol{x},t)}{\partial t} + \boldsymbol{V}(\boldsymbol{x}) \cdot \nabla \gamma(\boldsymbol{x},t) = 0, \tag{5}$$

where $D\gamma/Dt$ represents the material derivative and $\boldsymbol{V}(\boldsymbol{x})$ corresponds to the motion of the material coordinates, $\partial \boldsymbol{x}/\partial t$. The magnitude of the variations in shape can therefore be evaluated according to the magnitude of $\boldsymbol{V}(\boldsymbol{x})$ velocity. Considering the initial and boundary conditions for this fictitious advection equation, the uncertain shape variations are modeled as

$$\begin{cases} \frac{\partial \gamma(\boldsymbol{x},t)}{\partial t} + \boldsymbol{V}(\boldsymbol{x}) \cdot \nabla \gamma(\boldsymbol{x},t) = 0 & \text{for } (\boldsymbol{x},t) \in D \times [0,T] \\ \boldsymbol{n}(\boldsymbol{x}) \cdot \nabla \gamma(\boldsymbol{x},t) = 0 & \text{for } (\boldsymbol{x},t) \in \Gamma_- \times [0,T] \\ \gamma(\boldsymbol{x},0) = \overline{\gamma}(\boldsymbol{x}) & \text{for } \boldsymbol{x} \in D, \end{cases} \tag{6}$$

where T is a final time, $\boldsymbol{n}$ is a normal vector pointing outward and $\Gamma_- = \partial D|_{\boldsymbol{V} \cdot \boldsymbol{n} < 0}$. In the present study, we assume that the components of random velocity field $\boldsymbol{V}(\boldsymbol{x})$ are independent of each other and are Gaussian with a zero average. The Gaussian function is usually used to model a random error and has been applied to shape uncertainty modeling in the previous research (Jansen et al, 2013, 2015; Chen and Chen, 2011). Even though the Gaussian function is unbounded, it can also be used to model truncated normal distributions which are bounded, when the truncation occurs at the tail region (Ito et al, 2018). On the other hand, another assumption can be found in literature (Schevenels et al, 2011; Lazarov et al, 2012; Kang and Liu, 2018) in which the geometrical variations are represented by the random threshold projection and the probability density is assumed to be uniformly distributed in an interval.

3.2 Karhunen-Loève expansion

To express the random velocity field using uncorrelated random variables, we apply the Karhunen-Loève (K-L) expansion (Betz et al, 2014), a series expansion method that represents a continuous random field, $H(\boldsymbol{x}, \theta)$, as follows:

$$H(\boldsymbol{x},\theta) = \mu(\boldsymbol{x}) + \sum_{i=1}^{\infty} \sqrt{\lambda_i} \psi_i(\boldsymbol{x}) \xi_i(\theta), \tag{7}$$

where $\boldsymbol{x} \in D$ is a spatial coordinate, $\theta \in \Theta$ is a coordinate in the sample space Θ, $\mu(\boldsymbol{x})$ is the mean function of the random field, and ξ_i are standard normal mutually uncorrelated random variables. λ_i and ψ_i are the eigenvalue and eigenfunctions of the autocovariance function of the random field, obtained by solving the following homogeneous Fredholm integral equation of the second kind:

$$\int_D \text{Cov}(\boldsymbol{x},\boldsymbol{x}') \psi_i(\boldsymbol{x}') d\boldsymbol{x}' = \lambda_i \psi_i(\boldsymbol{x}), \tag{8}$$

where $\text{Cov}(\boldsymbol{x},\boldsymbol{x}')$ is an autocovariance function, modeled in this study using a Gaussian function as follows:

$$\text{Cov}(\boldsymbol{x},\boldsymbol{x}') = \sigma(\boldsymbol{x})\sigma(\boldsymbol{x}')\exp\left(\frac{\|\boldsymbol{x}-\boldsymbol{x}'\|^2}{l_C^2}\right), \tag{9}$$

where l_C is the correlation length and $\sigma(\boldsymbol{x})$ is the standard deviation at coordinate $\boldsymbol{x}$. Numerical methods for discretization of the continuous form of the eigenvalue problem in Eq. (8) were discussed in detail by Betz et al (2014). We use the finite element method to solve the problem, projecting the autocovariance function onto the space spanned by the shape function $\boldsymbol{N}$ as

$$\text{Cov}(\boldsymbol{x},\boldsymbol{x}') \approx \boldsymbol{N}(\boldsymbol{x})^{\text{T}} \boldsymbol{K} \boldsymbol{N}(\boldsymbol{x}'), \tag{10}$$

where $\boldsymbol{K}$ is the matrix whose components $k_{ij} = \text{Cov}(\boldsymbol{x}_i, \boldsymbol{x}_j)$ with $\boldsymbol{x}_i$ and $\boldsymbol{x}_j$ denoting the coordinates of the finite element nodes.
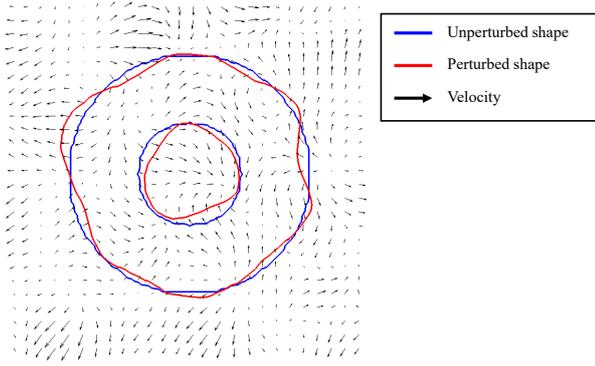
Fig. 2 A schematic of a perturbed shape by advection.

The above K-L expansion can then be approximated using a finite number of terms by sorting the eigenvalues λ_i and their corresponding eigenfunctions ψ_i in a descending order and truncating the series as follows:

$$H(\boldsymbol{x}, \theta) = \mu(\boldsymbol{x}) + \sum_{i=1}^{M} \sqrt{\lambda_i} \psi_i(\boldsymbol{x}) \xi_i(\theta), \tag{11}$$

where M is the number of terms of the truncated K-L expansion. The error due to the truncation can be evaluated as

$$\varepsilon_{\mathrm{KL}} = 1 - \frac{1}{\int_D \sigma(\boldsymbol{x})^2 d\Omega} \sum_{i=1}^{M} \lambda_i, \tag{12}$$

and set $\varepsilon_{\mathrm{KL}}$ is set as 0.1 in this study. Using the K-L expansion, the random velocity field can be approximated as

$$\boldsymbol{V}(\boldsymbol{x}, \theta) = \sum_{j=1}^{N} V_j(\boldsymbol{x}, \theta) \boldsymbol{e}_j = \sum_{j=1}^{N} \sum_{i=1}^{M} \sqrt{\lambda_i} \psi_i(\boldsymbol{x}) \xi_i^j(\theta) \boldsymbol{e}_j, \tag{13}$$

where $\boldsymbol{e}_j$ represents the basis vectors of the canonical coordinate and N is the number of spatial dimensions. Figure 2 illustrates a perturbed shape by the proposed geometrical uncertainty modeling using Eulerian description where the circular shape is perturbed by advection whose velocity is given by Eq. (13).

3.3 Inverse reliability method

Reliability can be theoretically defined as the probability of a desired state continuing in time, i.e., the probability of non-failure. The limit state of failure is represented as a function, g, called the limit state function, of stochastic variables $\boldsymbol{z}$ in which the safe state is represented as $g(\boldsymbol{z}) > 0$ and the failure state is $g(\boldsymbol{z}) < 0$. The isosurface of $g(\boldsymbol{z}) = 0$ is called the limit state surface. The probability of failure, P_f,
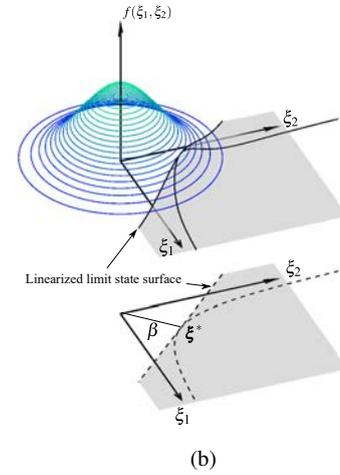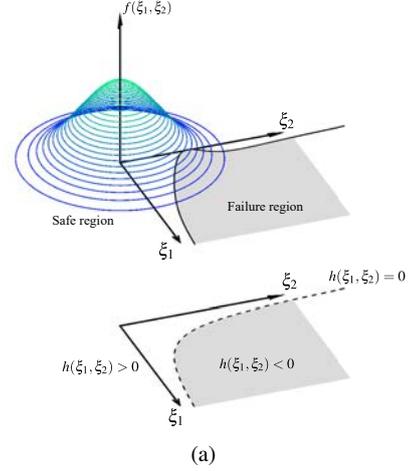

(a)

(b)

Fig. 3 Standard Gaussian probability density function: (a) limit state function; (b) linearized limit state function.

can be evaluated using the joint probability density function $f(\boldsymbol{z})$ and the limit state function $g(\boldsymbol{z})$ as follows:

$$P_f = \mathrm{P}(g(\boldsymbol{z}) < 0) = \int_{g(\boldsymbol{z})<0} f(\boldsymbol{z}) d\boldsymbol{z}. \tag{14}$$

Reliability P_r is evaluated as $P_r = 1 - P_f$. However, the complexity of $f(\boldsymbol{z})$ and $g(\boldsymbol{z})$ makes it computationally expensive to evaluate Eq. (14), so the first order reliability method (FORM) is often used, in which the limit state function is linearly approximated.

3.3.1 Reliability index approach

The FORM is usually used in a RIA. In a FORM, stochastic variables $\boldsymbol{z}$ are converted into independent standard Gaussian stochastic variables $\boldsymbol{\xi}$, and the limit state function in $\boldsymbol{\xi}$-space is then linearized at the design point, also called the most probable failure point (MPFP) $\boldsymbol{\xi}^*$, which is the nearest point on the limit state surface from the origin of

ξ-space. Figure 3 illustrates an example of a linearized limit state function in 2-D ξ-space where $h(\xi)$ is the limit state function in ξ-space. The probability of failure is then approximated using the standard Gaussian function, namely,

$$P_f = \Phi(-\beta) = \int_{-\infty}^{-\beta} \frac{1}{\sqrt{2\pi}} \exp\left(-\frac{1}{2}\xi^2\right) d\xi, \quad (15)$$

where β, called a reliability index, is the distance from the origin to the design point, obtained by solving the following problem:

$$\beta = \min_{\xi} \|\xi\| \text{ subject to } h(\xi) = 0. \quad (16)$$

The reliability constraint can then be imposed via β as

$$\beta \geq \Phi^{-1}(\overline{P_r}), \quad (17)$$

where $\overline{P_r}$ is the lower limit of reliability.

3.3.2 Performance measure approach

In contrast to a RIA, a performance measure approach (PMA) replaces a probabilistic constraint with a constraint with respect to the minimum performance on the hypersphere in ξ-space, which represents the target reliability index. That is, the point, called the minimum performance target point (MPTP), on a hypersphere of radius β_T where the limit state function is minimized, is searched using

$$h_{\min} = \min_{\xi} h(\xi) \text{ subject to } \|\xi\| = \beta_T = \Phi^{-1}(\overline{P_r}), \quad (18)$$

with the reliability constraint imposed as

$$h_{\min} \geq 0. \quad (19)$$

If reliability index β corresponds to target reliability index β_T, the most probable failure point (MPFP) corresponds to the MPTP.

In this study, shape uncertainty is represented using independent Gaussian random variables via an advection equation and K-L expansion, as mentioned previously in sections 3.1 and 3.2. Therefore, ξ-space is formed by setting

$$\xi = \left[\xi_1^1, \xi_2^1, \ldots, \xi_M^1, \xi_1^2, \ldots, \xi_M^N\right]. \quad (20)$$

4 Formulation of optimization problems

4.1 Minimum mean compliance problem

Consider that a traction t is applied to boundary Γ_t of a fixed design domain and displacement u is fixed at boundary Γ_u. We first consider a reliability-based topology optimization

for a mean compliance problem. That is, based on the mean compliance, the limit state function must be defined as

$$h(\xi) = c - \int_{\Gamma_t} t \cdot u d\Gamma, \quad (21)$$

where c is the threshold distinguishing a safe state from failure and the second term is the mean compliance which represents the elastic compliance of the structure against the applied force. However, the lack of local information such as stress makes it difficult to determine this threshold according to the mean compliance. In the previous study (Kang and Liu, 2018), this threshold was empirically determined. In the present study, on the other hand, we set the threshold as the objective function, instead of setting it in advance. The smaller the threshold value c is, the more the state is likely to become failure. Consequently, minimizing c under the reliability constraint yields the solution with maximum performance ensuring the target reliability index. Therefore, the optimization problem under a volume constraint can be formulated, as follows:

$$\inf_{\phi \in L^\infty(D;[-1,1])} J = c \quad (22)$$

subject to:

$$\min_{\xi \in S} \quad h(\xi, u, \phi) \geq 0, \quad (23)$$

$$\int_D \gamma(x, T) d\Omega - V_{\max} \leq 0, \quad (24)$$

with

$$h(\xi, u, \phi) = c - \int_{\Gamma_t} t \cdot u d\Gamma, \quad (25)$$

where S represents a hypersphere of radius β_T and $V_{\max}$ is the upper limit of the allowable volume. Assuming a linear elasticity for elastic tensor C and small strain tensor $\varepsilon(u) = (\nabla u + \nabla u^T)/2$, the displacement $u \in \mathscr{U}$ satisfies the following variational formulation:

$$\int_{\Gamma_t} t \cdot \tilde{u} d\Gamma - \int_D \varepsilon(\tilde{u}) : C\gamma(x, T)^p : \varepsilon(u) d\Omega = 0 \quad (26)$$

for all variables $\tilde{u} \in \mathscr{U}$, with space $\mathscr{U}$ defined as

$$\mathscr{U} = \{\tilde{u} \in H^1(D) \mid \tilde{u} = 0 \text{ on } \Gamma_u\}, \quad (27)$$

where H^1 is a Sobolev space.

4.2 Optimum design problem for a compliant mechanism

Consider again that a traction t is applied to boundary Γ_t of the fixed design domain and displacement u is fixed at boundary Γ_u. We now formulate a reliability-based topology optimization problem for the optimum design of a compliant mechanism. As was the case for the minimum mean compliance problem, the optimization problem is formulated by

setting the threshold of the limit state function as the objective function, as follows:

$$\inf_{\phi \in L^\infty(D;[-1,1])} \quad J = -c \tag{28}$$

subject to:

$$\min_{\boldsymbol{\xi} \in S} \quad h(\boldsymbol{\xi}, \boldsymbol{u}, \phi) \geq 0, \tag{29}$$

$$\int_D \gamma(\boldsymbol{x}, T) d\Omega - V_{\max} \leq 0, \tag{30}$$

with

$$h(\boldsymbol{\xi}, \boldsymbol{u}, \phi) = \int_{\Gamma_{\text{out}}} \boldsymbol{e} \cdot \boldsymbol{u} d\Gamma - c, \tag{31}$$

where Γ_{out} denotes the location where the displacement is to be maximized and $\boldsymbol{e}$ the direction in which the displacement is to be maximized. The first term in Eq. (31) is a mutual mean compliance which represents the elastic compliance of the structure for the desired direction $\boldsymbol{e}$ and is maximized in usual deterministic optimization. The larger the threshold value c in Eq. (31) is, the more the state is likely to become failure. Consequently, maximizing c under the reliability constraint yields the solution with maximum performance ensuring the target reliability index. Therefore, the optimization problem is formulated as a maximization problem by adding the minus sign to the objective function. Assuming a linear elasticity, displacement $\boldsymbol{u} \in \mathcal{U}$ satisfies the following variational formulation,

$$\int_{\Gamma_{\text{t}}} \boldsymbol{t} \cdot \tilde{\boldsymbol{u}} d\Gamma - \int_{\Gamma_{\text{t}}} k_{\text{in}} \boldsymbol{u} \cdot \tilde{\boldsymbol{u}} d\Gamma - \int_{\Gamma_{\text{out}}} k_{\text{out}} \boldsymbol{u} \cdot \tilde{\boldsymbol{u}} d\Gamma$$
$$- \int_D \varepsilon(\tilde{\boldsymbol{u}}) : \boldsymbol{C} \gamma(\boldsymbol{x}, T)^p : \varepsilon(\boldsymbol{u}) d\Omega = 0 \tag{32}$$

for all variables $\tilde{\boldsymbol{u}} \in \mathcal{U}$, where k_{in} and k_{out} are parameters for Robin boundary conditions imposed to ensure the stiffness of the obtained configurations.

4.3 Sensitivity analysis

Here, sensitivities for the MPTP search and updating of the design variables are derived based on the adjoint variable method for the following problem:

$$\inf_{\phi \in L^\infty(D;[-1,1])} \quad J = c \tag{33}$$

with a reliability constraint

$$\min_{\boldsymbol{\xi} \in S} \quad h(\boldsymbol{\xi}, \boldsymbol{u}, \phi) \geq 0, \tag{34}$$

where

$$h(\boldsymbol{\xi}, \boldsymbol{u}, \phi) = c - \left(\int_D f_{\text{d}}(\boldsymbol{u}, \eta(\boldsymbol{x}, T)) d\Omega + \int_{\partial D} f_{\text{b}}(\boldsymbol{u}) d\Gamma \right). \tag{35}$$

This problem is equivalent to the following min-max problem:

$$\inf_{\phi \in L^\infty(D;[-1,1])} \quad J = \max_{\boldsymbol{\xi} \in S} \int_D f_{\text{d}}(\boldsymbol{u}, \eta(\boldsymbol{x}, T)) d\Omega + \int_{\partial D} f_{\text{b}}(\boldsymbol{u}) d\Gamma, \tag{36}$$

so the sensitivity analysis is performed to the above formulation. With the equality constraints comprised of the governing equation for linear elasticity, the fictitious advection equation, and the PDE-filter, the Lagrangian is defined as

$$L\left(\phi, \xi_i^j, \zeta, \overline{\eta}, \eta, \boldsymbol{v}, \tilde{\zeta}, \tilde{\eta}_{\text{H}}, \tilde{\eta}_0 \tilde{\eta}, \tilde{\boldsymbol{v}} \right)$$
$$= \int_D f_{\text{d}}(\boldsymbol{v}, \eta(\boldsymbol{x}, T)) d\Omega + \int_{\partial D} f_{\text{b}}(\boldsymbol{v}) d\Gamma$$
$$+ \int_{\Gamma_{\text{t}}} \boldsymbol{t} \cdot \tilde{\boldsymbol{v}} d\Gamma - \int_D \varepsilon(\tilde{\boldsymbol{v}}) : \boldsymbol{C} \eta(\boldsymbol{x}, T)^p : \varepsilon(\boldsymbol{v}) d\Omega$$
$$- \text{A} \left[\int_{\Gamma_{\text{t}}} k_{\text{in}} \tilde{\boldsymbol{v}} \cdot \boldsymbol{v} d\Gamma + \int_{\Gamma_{\text{out}}} k_{\text{out}} \tilde{\boldsymbol{v}} \cdot \boldsymbol{v} d\Gamma \right]$$
$$+ \int_0^T \int_D \tilde{\eta} \left(\frac{\partial \eta}{\partial t} + \boldsymbol{V} \cdot \nabla \eta \right) d\Omega dt$$
$$+ \int_D \tilde{\eta}_0 \left(\eta(\boldsymbol{x}, 0) - \overline{\eta} \right) d\Omega$$
$$+ \int_D \tilde{\eta}_{\text{H}} (\overline{\eta} - H_\alpha(\zeta)) d\Omega$$
$$+ \int_D \left(\tilde{\zeta} \phi - R^2 \nabla \tilde{\zeta} \cdot \nabla \zeta - \tilde{\zeta} \zeta \right) d\Omega, \tag{37}$$

where ζ, $\overline{\eta}$, η, $\boldsymbol{v}$, $\tilde{\zeta}$, $\tilde{\eta}_{\text{H}}$, $\tilde{\eta}_0$, $\tilde{\eta}$ and $\tilde{\boldsymbol{v}}$ are variables that are independent of ϕ and ξ_i^j. $\text{A} = 0$ for the minimum mean compliance problem, and $\text{A} = 1$ for the optimum design problem for a compliant mechanism. The design sensitivity can be derived by taking the necessary conditions for optimality of the Lagrangian with respect to these variables. First, setting the Gâteaux derivative of the Lagrangian equal to zero with respect to variables $\tilde{\zeta}$, $\tilde{\eta}_{\text{H}}$, $\tilde{\eta}_0$, $\tilde{\eta}$ and $\tilde{\boldsymbol{v}}$ yields the stationary conditions for $\zeta = \varphi$, $\overline{\eta} = \overline{\gamma}$, $\eta = \gamma$ and $\boldsymbol{v} = \boldsymbol{u}$, respectively. Next, setting the Gâteaux derivative of the Lagrangian equal to zero with respect to variables ζ, $\overline{\eta}$, η and $\boldsymbol{v}$ at the optimal point for $\tilde{\zeta}$, $\tilde{\eta}_{\text{H}}$, $\tilde{\eta}_0$, $\tilde{\eta}$ and $\tilde{\boldsymbol{v}}$ yields the stationary conditions for $\tilde{\zeta} = \varphi_{\text{A}}$, $\tilde{\eta} = \gamma_{\text{A}}$, $\tilde{\eta}_{\text{H}} = \tilde{\eta}_0 = \gamma_{\text{A}}(\boldsymbol{x}, 0)$ and $\tilde{\boldsymbol{v}} = \boldsymbol{u}_{\text{A}}$, where $\boldsymbol{u}_{\text{A}}$, γ_{A} and φ_{A} are the solutions of the following adjoint equations.

Adjoint equation for linear elasticity:

$$\int_D \frac{\partial f_{\text{d}}(\boldsymbol{u}, \gamma)}{\partial \boldsymbol{u}} \cdot \tilde{\boldsymbol{u}}_{\text{A}} d\Omega + \int_{\partial D} \frac{\partial f_{\text{b}}(\boldsymbol{u})}{\partial \boldsymbol{u}} \cdot \tilde{\boldsymbol{u}}_{\text{A}} d\Gamma$$
$$- \text{A} \left[\int_{\Gamma_{\text{t}}} k_{\text{in}} \tilde{\boldsymbol{u}}_{\text{A}} \cdot \boldsymbol{u}_{\text{A}} d\Gamma + \int_{\Gamma_{\text{out}}} k_{\text{out}} \tilde{\boldsymbol{u}}_{\text{A}} \cdot \boldsymbol{u}_{\text{A}} d\Gamma \right]$$
$$- \int_D \varepsilon(\tilde{\boldsymbol{u}}_{\text{A}}) : \boldsymbol{C} \gamma(\boldsymbol{x}, T)^p : \varepsilon(\boldsymbol{u}_{\text{A}}) d\Omega = 0 \tag{38}$$

for all variables $\tilde{\boldsymbol{u}}_{\text{A}} \in \mathcal{U}$. This adjoint equation is conventional except that the advected normalized density $\gamma(\boldsymbol{x}, T)$ is

used.

Adjoint equation for fictitious advection equation:

$$
\begin{cases}
-\dfrac{\partial \gamma_{\mathrm{A}}}{\partial t} - \nabla \cdot (\boldsymbol{V} \gamma_{\mathrm{A}}) = 0 & \text{for } (\boldsymbol{x}, t) \in D \times [0, T] \\
\gamma_{\mathrm{A}}(\boldsymbol{x}, t) = 0 & \text{for } (\boldsymbol{x}, t) \in \Gamma_+ \times [0, T] \\
\gamma_{\mathrm{A}}(\boldsymbol{x}, T) = p \boldsymbol{\varepsilon}(\boldsymbol{u}_{\mathrm{A}}) : \boldsymbol{C} \gamma^{(p-1)} : \boldsymbol{\varepsilon}(\boldsymbol{u}) - \dfrac{\partial f_{\mathrm{d}}(\boldsymbol{u}, \gamma)}{\partial \gamma} \\
& \text{for } \boldsymbol{x} \in D,
\end{cases}
\tag{39}
$$

where $\Gamma_+ = \partial D|_{\boldsymbol{V} \cdot \boldsymbol{n} > 0}$. This is a retrograde advection equation with respect to time and velocity, starting from final time T, and the initial condition given at time T is a conventional sensitivity for density approaches in topology optimization. Therefore, this adjoint equation represents the sensitivity mapping from a perturbed (advected) shape to an unperturbed shape.

Adjoint equation for Helmholtz-type of PDE filter:

$$
-R^2 \nabla^2 \varphi_{\mathrm{A}} + \varphi_{\mathrm{A}} = -\gamma_{\mathrm{A}}(\boldsymbol{x}, 0) \frac{dH_\alpha}{d\varphi}.
\tag{40}
$$

This adjoint equation implies that the PDE filter will also be applied to sensitivities $\gamma_{\mathrm{A}}(\boldsymbol{x}, 0) dH_\alpha / d\varphi$. The gradient of performance function h then corresponds to the gradient of the Lagrangian with respect to ξ_i^j at the optimal point for ζ, $\overline{\eta}$, η, $\boldsymbol{v}$, $\tilde{\zeta}$, $\tilde{\eta}_{\mathrm{H}}$, $\tilde{\eta}_0$, $\tilde{\eta}$ and $\tilde{\boldsymbol{v}}$, calculated as

$$
\frac{\partial h}{\partial \xi_i^j} = \frac{\partial L}{\partial \xi_i^j} = \int_0^T \int_D \gamma_{\mathrm{A}} \lambda_i \psi_i \boldsymbol{e}_j \cdot \nabla \gamma \, d\Omega dt.
\tag{41}
$$

This gradient is used to obtain the MPTP. Finally, the design sensitivity, i.e., the gradient of the objective functional with respect to ϕ, is equal to the Gâteaux derivative of the Lagrangian with respect to ϕ at the optimal point for ζ, $\overline{\eta}$, η, $\boldsymbol{v}$, $\tilde{\zeta}$, $\tilde{\eta}_{\mathrm{H}}$, $\tilde{\eta}_0$, $\tilde{\eta}$, $\tilde{\boldsymbol{v}}$ and $\boldsymbol{\xi}$, preceded by a minus sign, as follows:

$$
\langle J', \delta\phi \rangle = -dL(\phi; \delta\phi) = -\int_D \varphi_{\mathrm{A}} \delta\phi \, d\Omega,
\tag{42}
$$

where $dL(\phi; \delta\phi)$ represents the Gâteaux derivative of the Lagrangian with respect to ϕ in the $\delta\phi$ direction.

4.4 Filtering of the standard deviation function

The proposed method expresses shape variations using an advection scheme. If locations where loads are applied are allowed to be perturbed, the influence of shape variations on the loading conditions must be considered. For simplicity in the present study, we assume that variations in the boundaries where the loads are applied are very small, i.e., the

standard deviation $\sigma(\boldsymbol{x})$ is sufficiently small at these boundaries. For numerical stability, the standard deviation $\sigma(\boldsymbol{x})$ for the entire domain is calculated using the Helmholtz-type of PDE filter, as follows:

$$
\int_D \left(\tilde{\sigma}\sigma_0 - l_\sigma^2 \nabla\tilde{\sigma} \cdot \nabla\sigma - \tilde{\sigma}\sigma \right) d\Omega = 0
\tag{43}
$$

for $\sigma \in \mathfrak{S}$ and all variables $\tilde{\sigma} \in \tilde{\mathfrak{S}}$, with

$$
\mathfrak{S} = \{ \sigma \in H^1(D) \mid \tilde{\sigma} = \sigma_0 \varepsilon \text{ on } \Gamma_\sigma \}
\tag{44}
$$

$$
\tilde{\mathfrak{S}} = \{ \tilde{\sigma} \in H^1(D) \mid \tilde{\sigma} = 0 \text{ on } \Gamma_\sigma \},
\tag{45}
$$

where l_σ is a parameter determining the degree of smoothing, σ_0 is the characteristic standard deviation, and ε is a sufficiently small positive number, set as 10^{-4} in this study. Since the magnitude of $\sigma(\boldsymbol{x})$ is determined by that of σ_0, the parameter σ_0 determines the degrees of the standard deviation for the shape uncertainty. Consequently, this value should be adjusted to represent the standard deviation in the certain manufacturing process or usage environment which is focused on. However, this paper focuses on the construction of a reliability-based topology optimization under shape uncertainty and does not focus on the particular manufacturing process or usage environment. Therefore, this parameter is empirically determined to $\sigma_0 = 2$ in the present study. The parameter l_σ is also empirically set to $0.1L$ where L is the characteristic length of the design domain. $\Gamma_\sigma = \Gamma_{\mathrm{t}}$ for the minimum mean compliance problem, and $\Gamma_\sigma = \Gamma_{\mathrm{t}} \cup \Gamma_{\mathrm{out}}$ for the compliant mechanism optimum design problem.

5 Numerical implementation

5.1 MPTP search algorithm

Several methods have been proposed to search for the MPTP during the inner loop of the optimization procedure, such as the advanced mean value, conjugate mean value, and hybrid mean value methods (Youn et al, 2003), the conjugate gradient method (Ezzati et al, 2015), and hybrid chaos control method (Meng et al, 2015). In the present study, to stably handle geometrical uncertainties that yield highly nonlinear limit state functions, we introduce a step size, s, into the advanced mean value method, in a manner similar to the scheme adopted in previous research (Keshtegar and Lee, 2016), and use the following update formula:

$$
\boldsymbol{\xi}^n = \beta_{\mathrm{T}} \frac{\tilde{\boldsymbol{\xi}}^n}{\|\tilde{\boldsymbol{\xi}}^n\|_{L^2}}
\tag{46}
$$

with

$$
\tilde{\boldsymbol{\xi}}^n = (1-s)\boldsymbol{\xi}^{n-1} - s\beta_{\mathrm{T}} \frac{\nabla_{\boldsymbol{\xi}} h(\boldsymbol{\xi}^{n-1}, \boldsymbol{u}, \phi)}{\|\nabla_{\boldsymbol{\xi}} h(\boldsymbol{\xi}^{n-1}, \boldsymbol{u}, \phi)\|_{L^2}},
\tag{47}
$$

where $\boldsymbol{\xi}^n$ represents $\boldsymbol{\xi}$ at the nth inner iteration. When $s = 1$, the above update formula corresponds to that used in the advanced mean value method. The following is the MPTP search algorithm we employ:

Step 1 Set the initial value of $\boldsymbol{\xi}$ as $\boldsymbol{\xi}^0 = \mathbf{0}$ and the iteration counter with $n = 1$.

Step 2 Set the step size as $s = 1$.

Step 3 Solve the advection equation in Eq. (6) with the finite difference method.

Step 4 Solve the governing equation with the finite element method.

Step 5 Compute a new value for performance function h^{n+1}.

Step 6 If $h^{n+1} > h^n$, then set $s \leftarrow 0.5s$ and proceed to Step 8. Otherwise set $s = 1$, $n \leftarrow n+1$ and proceed to Step 7.

Step 7 Compute the sensitivities of the performance function based on the adjoint variable method, as explained below.

Step 8 Update $\boldsymbol{\xi}$ using the update formula in Eq. (46).

Step 9 If the change in $\boldsymbol{\xi}$ is sufficiently small and satisfies

$$\frac{\|\boldsymbol{\xi}^n - \boldsymbol{\xi}^{n-1}\|_{L^2}}{\beta_\mathrm{T}} \leq \varepsilon_\mathrm{inner}, \tag{48}$$

the MPTP search halts, otherwise return to Step 3.

Due to the local search strategy, this algorithm can obtain only one solution even if there are several MPTP points. However, the local search-based reliability analysis is still a powerful approach to obtain a candidate of the MPTP efficiently and has widely been used in previous research (Keshtegar and Lee, 2016; Kang and Liu, 2018). We hope to address the issue in our future research.

5.2 Optimization algorithm

The optimization algorithm is now described:

Step 1 Perform the K-L expansion with the finite element method to obtain ψ_i and λ_i for $i = 1, 2, \ldots, M$, where M is determined as the minimum value satisfying $\varepsilon_\mathrm{KL} \leq \overline{\varepsilon_\mathrm{KL}}$. $\overline{\varepsilon_\mathrm{KL}}$ is the allowable error of the truncated K-L expansion.

Step 2 Set initial values for ϕ.

Step 3 Apply the PDE filter to ϕ with the finite element method.

Step 4 Perform the MPTP search in the inner loop as described above.

Step 5 Compute the design sensitivity based on the adjoint variable method as described in the next section.

Step 6 Update the design variables ϕ using the method of moving asymptotes (MMA) (Svanberg, 1987).

Step 7 If the change in the design variables is sufficiently small and satisfies

$$\frac{\|\phi^n - \phi^{n-1}\|_{L^2(D)}}{\|\phi^n\|_{L^2(D)}} \leq \varepsilon_\mathrm{opt}, \tag{49}$$

where ϕ^n represents ϕ at the nth outer iteration, the optimization procedure halts, otherwise return to Step 3.

In the present study, to achieve an almost 0–1 density in the optimized solutions, the continuation scheme is applied. In the continuation scheme, parameter α for the Heaviside projection was initially set to 10. Once the optimization procedure converged, the parameter was increased by 5 and the optimization procedure restarted. This continuation scheme was applied until the parameter α reached 25. The convergence criteria for the inner and outer loops were set with $\varepsilon_\mathrm{inner} = 1 \times 10^{-4}$ and $\varepsilon_\mathrm{opt} = 1 \times 10^{-3}$, respectively.

6 Numerical examples

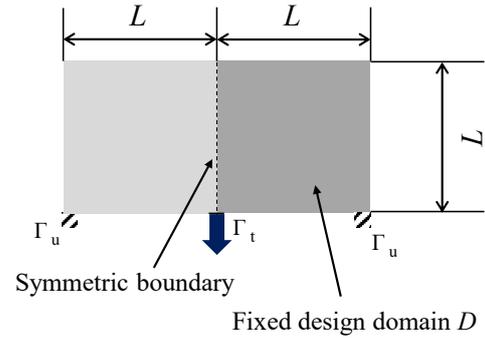### 6.1 Verification by Monte Carlo Simulation

Fig. 4 Fixed design domain and boundary conditions for bridge design problem.

First, the accuracy of the PMA is examined by comparing the failure probability estimated by the proposed method and the Monte Carlo Simulation (MCS), via the minimum mean compliance problem formulated in Section 4.1. To make the failure probability estimated by the MCS be sufficiently close to the true value, more random samples are required as the true failure probability gets smaller. That is, the larger the target reliability index is in the PMA, the more iterations in the MCS would be required to verify the accuracy of the PMA by the MCS. In terms of the computational cost of the MCS, we set β_T up to 3 for comparison, and 10^5 samples were used for each MCS.

Figure 4 shows the fixed design domain and boundary conditions. Since the design model is symmetrical, only the right half was considered as the design domain. For application of the finite element method, the design domain was discretized into 200×100 first-order quadrilateral elements. When applying the finite difference method, the Lax-Wendroff
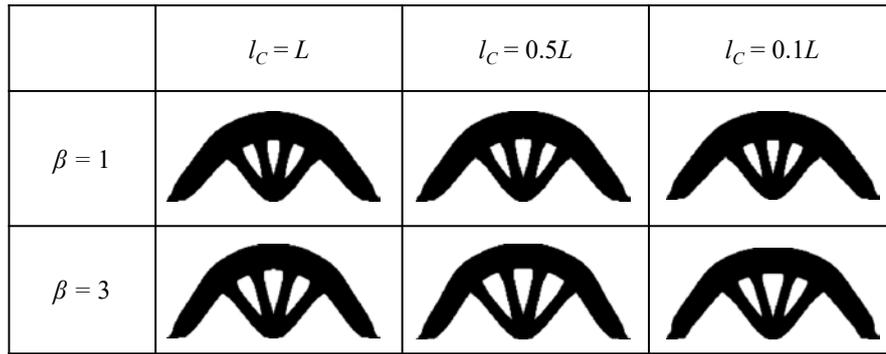
	$l_C = L$	$l_C = 0.5L$	$l_C = 0.1L$
$\beta = 1$			
$\beta = 3$			

Fig. 5 Obtained optimized configurations.

Table 1 Comparison between PMA and MCS.

β_T values for optimization	Case 1 where $l_C = L$		Case 2 where $l_C = 0.5L$		Case 3 where $l_C = 0.1L$	
	β_{MCS}	$\widehat{Cov}$	β_{MCS}	$\widehat{Cov}$	β_{MCS}	$\widehat{Cov}$
1.0	0.50	4.8×10^{-3}	0.29	4.0×10^{-3}	-0.60	1.9×10^{-3}
1.5	1.08	7.9×10^{-3}	0.88	6.6×10^{-3}	-0.10	2.9×10^{-3}
2.0	1.61	1.3×10^{-2}	1.38	1.0×10^{-2}	0.36	4.2×10^{-3}
2.5	2.00	2.1×10^{-2}	1.79	1.6×10^{-2}	0.82	6.2×10^{-3}
3.0	2.32	3.1×10^{-2}	2.11	2.4×10^{-2}	1.30	9.7×10^{-3}

method was used, which is an explicit scheme and is suitable for straightforward parallel computation. For application of the Lax-Wendroff scheme, the fixed design domain was discretized into a 201×101 grid, with spatial steps in both directions of $\Delta x = 1.0$ and time steps of $\Delta t = \min(0.2, 0.5\Delta t_{CFL})$, where Δt_{CFL} is the maximum time step satisfying the CFL condition. The minmod function was adopted as the flux limiter. The upper limit of the allowable volume was set to 40% of the volume of the fixed design domain. The PDE filter parameter was set to $R = 1.5$. The final time for the advection was set to $T = 1$, which implies that the magnitude of velocity $\boldsymbol{V}(\boldsymbol{x})$ represents the magnitude of the shape variations. In other words, the standard deviation of the shape variation at each point is approximately $\sigma(\boldsymbol{x})$.

Figure 5 illustrates some of the optimized configurations obtained for various values of β_T and l_C. All configurations have the same topology, but the size of the interior voids is different depending on the parameter settings. Table 1 lists the reliability index β_{MCS} calculated by the MCS performed to the optimized configurations obtained by the proposed method, and the coefficient of variation on the estimated failure probability, $\widehat{Cov}$. Since the coefficient of variation on the estimated failure probability, $\widehat{Cov}$, is sufficiently small, it is confirmed that the failure probability calculated by the MCS is close to the true value. This table implies that the PMA overestimates the reliability. This would be resulted from high nonlinearity of the limit state function on the geometrical variations. However, the relative relation of the reliability index between the PMA and the MCS agrees

with each other. Therefore, the proposed method using the the PMA can efficiently and qualitatively consider the reliability. More accurate reliability would be obtained by using a higher order analysis such as the second-order reliability method (SORM).

The computational time in the reliability analysis is investigated in this example. The finite element analysis to compute the limit state value was dominant in the reliability analysis. On the other hand, that of the advection equation was only up to 11%.

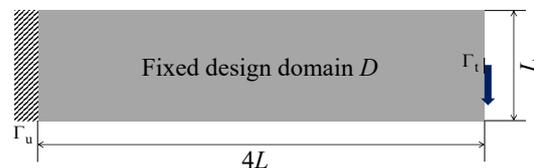### 6.2 Cantilever design problem

Fig. 6 Fixed design domain and boundary conditions for cantilever design problem.

Now, the proposed method is applied to the cantilever design problem based on the formulation in Section 4.1. Figure 6 shows the fixed design domain and boundary conditions. For application of the finite element method, the fixed design domain was discretized into 320×80 first-order

quadrilateral elements. For application of the Lax-Wendroff scheme, the fixed design domain was discretized into a 321×81 grid, with spatial steps in both directions of $\Delta x = 1.0$ and time steps of $\Delta t = \min{(0.2, 0.5 \Delta t_{\text{CFL}})}$, where Δt_{CFL} is the maximum time step satisfying the CFL condition. The upper limit of the allowable volume was set to 50% of the volume of the fixed design domain. The PDE filter parameter was set to $R = 2.5$. The final time for the advection was set to $T = 1$.

6.2.1 Dependency of optimal configuration on parameter β_T
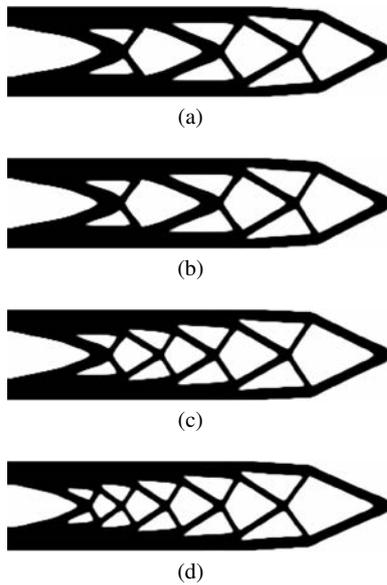
Fig. 7 Obtained optimized configurations for (a) $\beta_T = 0$ (deterministic solution); (b) $\beta_T = 1$; (c) $\beta_T = 3$; and (c) $\beta_T = 5$.

Table 2 Mean compliance values ($\times 10^4$) at MPTP calculated by setting various values of β_T for optimized configurations shown in Fig. 7 after optimization.

β_T values for analysis	β_T values for optimization			
	0	1	3	5
0	3.50	3.50	3.50	3.52
1	3.68	3.66	3.66	3.67
3	4.04	4.02	3.99	3.99
5	4.58	4.52	4.41	4.34

Here, we examine the dependency of obtained optimized configurations on parameter β_T that represents the target reliability index. In these examples, parameter l_C in Eq. (9) that determines the autocorrelation in the K-L expansion
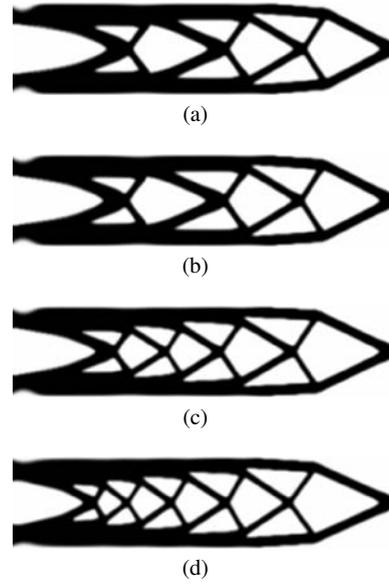

Fig. 8 Perturbed shapes at MPTP when setting $\beta_T = 5$ for optimized configurations obtained with (a) $\beta_T = 0$; (b) $\beta_T = 1$; (c) $\beta_T = 3$; and (d) $\beta_T = 5$.

was set to $0.1L$, resulting in $M = 325$. This value is relatively large due to the small correlation length setting.

Figure 7 shows the obtained optimized configurations for various values of β_T. As β_T is increased, the obtained optimized configurations include thicker elements near the fixed boundary and an increasing number of linear elements, which implies that considering geometrical variations in topology optimization is more important when the target reliability is large. Table 2 lists the mean compliance values at MPTPs calculated after optimization by setting various values for β_T for each optimized configuration obtained when $\beta_T = 0, 1, 3$, and 5. The data show that when $\beta_T \leq 1$ for post-analysis, the values of the objective function are almost the same as those for optimized configurations obtained when $\beta_T = 0, 1, 3$, and 5. On the other hand, as β_T for post-analysis is increased, optimized configurations obtained for each β_T are superior to those obtained for other β_T values in this optimization. This indicates that the proposed method can effectively obtain local optima that have some degree of reliability for geometrical variations, depending on the β_T setting.

Figure 8 shows the perturbed shapes at MPTPs calculated by setting $\beta_T = 5$ after optimization for each of the optimized configurations shown in Fig. 7. The linear elements near the fixed boundary become very thin when $\beta_T \leq 3$, whereas this thinning was alleviated when $\beta_T = 5$, which results in a high stiffness for shape variations (Fig. 8).
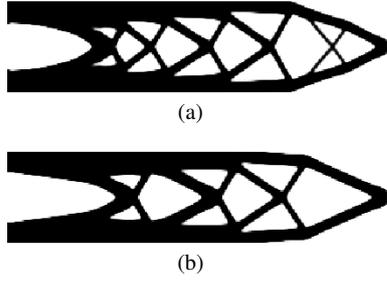
Fig. 9 Obtained optimized configurations for (a) $l_C = 0.5L$; and (b) $l_C = L$.
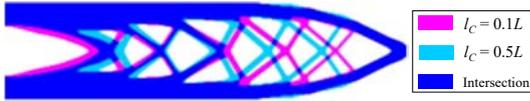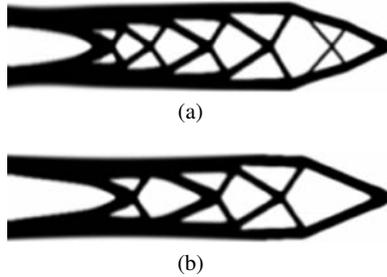

Fig. 10 Overlay image highlighting differences between optimized configurations obtained for $l_C = 0.1L$ and $0.5L$.

Table 3 Mean compliance values ($\times 10^4$) at MPTPs calculated with $l_C = 0.1L, 0.5L$, and L for optimized configurations shown in Fig. 9 after optimization.

l_C values for analysis	l_C values for optimization		
	$0.1L$	$0.5L$	L
$0.1L$	4.34	4.65	4.84
$0.5L$	5.03	5.02	5.24
L	4.99	4.99	4.91

Fig. 11 Perturbed shapes at MPTPs when setting $\beta_T = 5$ for optimized configurations obtained with (a) $l_C = 0.5L$; and (b) $l_C = L$.

6.2.2 Dependency of optimal configuration on parameter l_C

Next, we examine the dependency of obtained optimized configurations on parameter l_C in Eq. (9), which determines the spatial width of the autocorrelation function for geometrical variations. In this example, parameter β_T was set to 5 and two cases were examined, with $l_C = 0.5L$ resulting in $M = 17$, and $l_C = L$ resulting in $M = 6$.

Figure 9 shows the optimized configurations obtained for $l_C = 0.5L$ and L. Although the optimized configurations for $l_C = 0.5L$ (Fig. 9(a)) and $l_C = 0.1L$ (Fig. 7(d)) have the same topology, there are geometrical differences. The op-

timized configuration when $l_C = 0.1L$ has thicker elements near the boundary where the design domain is fixed than when $l_C = 0.5L$, as shown in Fig. 10. On the other hand, the optimized configuration with $l_C = L$ has fewer linear elements than when $l_C = 0.1L$ or $0.5L$, and is similar to the deterministic solution, which implies that considering geometrical uncertainty in topology optimization is more important when the correlation length of the variations is small.

Table 3 lists mean compliance values at the MPTPs calculated after optimization, with settings of $l_C = 0.1L, 0.5L$, and L for each optimized configuration obtained when $l_C = 0.1L, 0.5L$, and L. Here, the data show that the optimized configuration obtained for a certain value of l_C has the lowest mean compliance among the optimized configurations obtained for other values of l_C with respect to a given l_C setting used for post-analysis. This demonstrates that the proposed method effectively obtains solutions when various l_C settings are applied.

Figure 11 illustrates the perturbed shapes at MPTPs for optimized configurations obtained when $l_C = 0.5L$ and L (Fig.9). Compared with the perturbed shapes for the optimized configurations when $l_C = 0.1L$, the upper and lower frames have become uniformly thin, reflecting the larger width of the autocorrelation function when $l_C = 0.5L$ and L. Thus, parameter l_C values have a significant effect on considered shape variations and resulting optimal configurations, and therefore should be carefully set to harmonize with a particular manufacturing situation or usage environment.

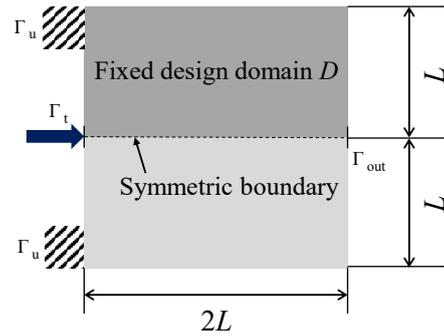### 6.3 Optimum design problem for a compliant mechanism

Fig. 12 Fixed design domain and boundary conditions for compliant mechanism optimum design problem.

Last, the proposed method is applied to an optimum design problem for the compliant mechanism problem formulated in Section 4.2. Figure 12 shows the fixed design domain and boundary conditions. Since the design model is symmetrical, only the upper half was considered as the design domain. For the finite element method analysis, the
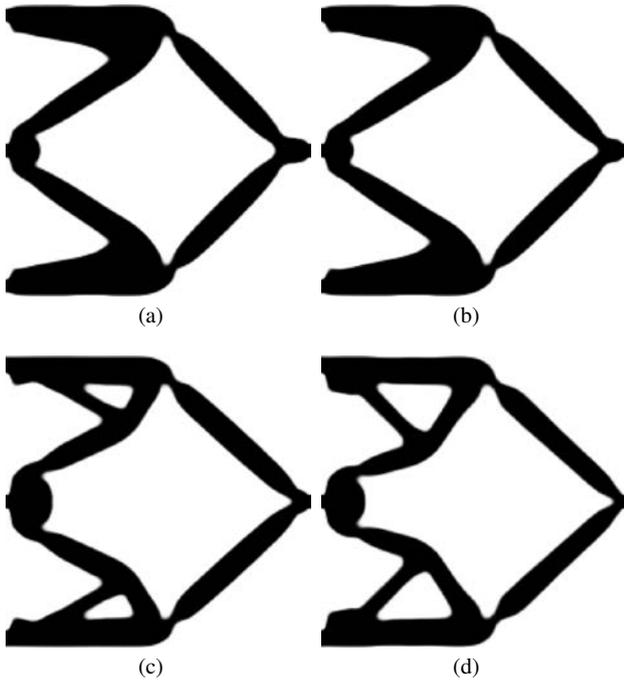
Fig. 13 Obtained optimized configurations for (a) $\beta_T = 0$ (deterministic solution); (b) $\beta_T = 1$; (c) $\beta_T = 3$ and (b) $\beta_T = 5$.

Table 4 Mutual mean compliance values at MPTPs calculated with various values of β_T for optimized configurations shown in Fig. 13 after optimization.

β_T values for analysis	β_T values for optimization			
	0	1	3	5
0	1.22	1.21	1.20	1.20
1	1.14	1.14	1.14	1.13
3	0.84	0.84	0.88	0.87
5	0.35	0.34	0.40	0.53

fixed design domain was discretized into 200×100 first-order quadrilateral elements. The Lax-Wendroff scheme was used for the finite difference method analysis, with the fixed design domain discretized into a 201×101 grid, with spatial steps of $\Delta x = 1.0$ in both directions, and a time step of $\Delta t = \min (0.2, 0.5 \Delta t_{\text{CFL}})$. The minmod function was adopted as the flux limiter. The upper limit of the allowable volume was set to 30% of the fixed design domain volume. The PDE filter parameter was set to $R = 5.0$. The final time for the advection was set to $T = 1$, which implies that the magnitude of velocity $V(x)$ represents the magnitude of shape variations. Parameters for the Robin boundary conditions were set with $k_{\text{in}} = 1.0$ and $k_{\text{out}} = 0.01$.

6.3.1 Dependency of optimal configuration on parameter β_T
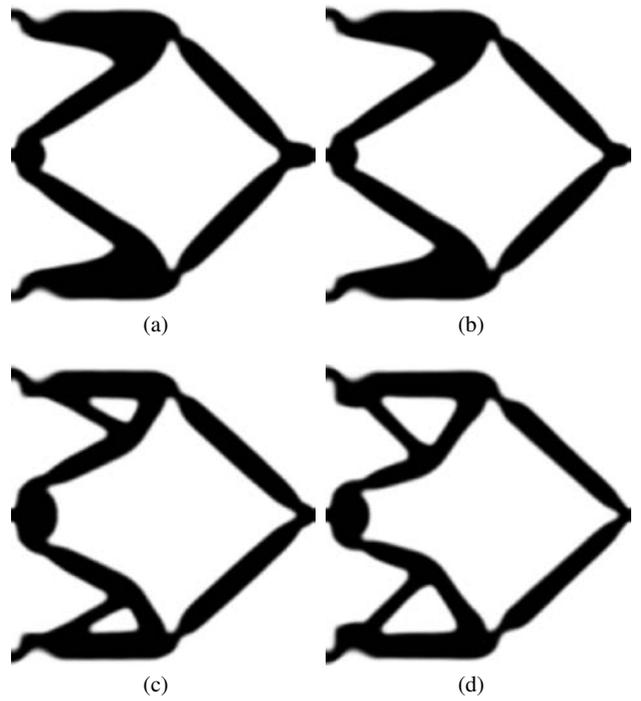

Fig. 14 Perturbed shapes at MPTPs when setting $\beta_T = 5$ for optimized configurations obtained when (a) $\beta_T = 0$ (deterministic solution); (b) $\beta_T = 1$; (c) $\beta_T = 3$ and (b) $\beta_T = 5$.

In this subsection, we again examined the dependency of obtained optimized configurations on parameter β_T that represents the target reliability index. The parameter for the K-L expansion was set to $l_C = l_\sigma = 0.1L$, which resulted in $M = 162$.

Figure 13 shows the obtained optimized configurations for the various values of β_T. These configurations have different topologies, and as the value of β_T is increased, the corresponding optimized configurations have thicker elements near the boundaries where the displacement is fixed or the traction is applied. This behavior is similar to that in the minimum mean compiliance problem. Again, we confirmed that considering geometrical variations in topology optimization is important when the target reliability is large. Table 4 lists the mutual mean compliance values at MPTPs calculated after optimization, having set various values of β_T for each optimized configuration shown in Fig. 13. The data indicate that the optimized configuration obtained for a certain value of β_T has the highest mutual mean compliance, i.e., a lower value of the objective function, among the optimized configurations obtained for other values of β_T with respect to a given β_T setting for post-analysis. The proposed method thus can obtain optimal configurations with higher reliability for geometrical variations, depending on the β_T setting, although the deterministic value of the mutual mean compliance is degraded.

Figure 14 shows the perturbed shapes at MPTPs calculated by setting $\beta_T = 5$ after optimization for each of the optimized configurations shown in Fig. 13. The results show that the elements near the fixed boundary have become much thinner, for all configurations, and the optimized configuration obtained when $\beta_T = 3$, and 5 has an additional supporting structure that provides increased reliability for shape variations. Note that shape variations illustrated in Figs. 14(a)–(d) mainly occurred at the elements near the fixed boundary, and these variations did not make any hinges in compliant mechanism designs. This means that the proposed method works similarly to the deterministic one for hinges, in this example. Consequently, the proposed method does not ensure the hinge-less designs, and the appropriate settings of parameters for the Robin boundary conditions, corresponding to the spring stiffness, prevented hinges from appearing in the optimized solutions.

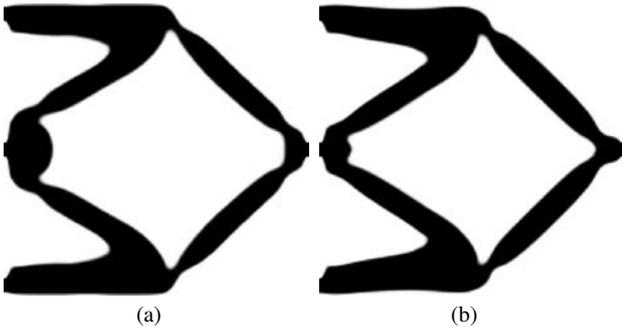### 6.3.2 Dependency of optimal configuration on parameter l_C

Fig. 15 Obtained optimized configurations for (a) $l_C = 0.5L$; and (b) $l_C = L$.

Table 5 Mutual mean compliance values at MPTPs calculated with $l_C = 0.1L, 0.5L$, and L for optimized configurations shown in Fig. 15 after optimization.

l_C values for analysis	l_C values for optimization		
	0.1L	0.5L	L
0.1L	0.88	0.72	0.74
0.5L	0.81	0.90	0.90
L	0.98	0.93	1.04

Here, we examine the dependency of obtained optimized configurations on parameter l_C. In this example, parameter β_T was set to 5 and two cases were examined, with $l_C = 0.5L$ resulting in $M = 9$, and $l_C = L$ resulting in $M = 4$.

Figure 15 illustrates the optimized configurations obtained for $l_C = 0.5L$ and L. The optimized configurations
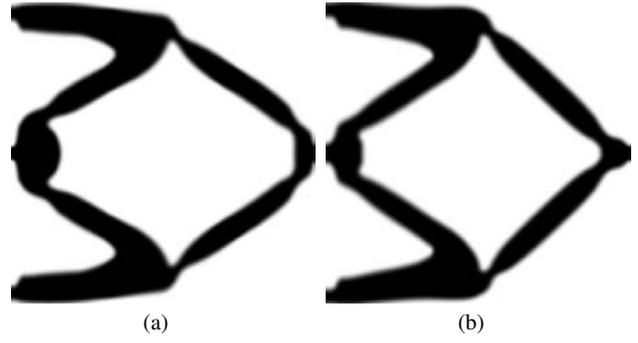

Fig. 16 Perturbed shapes at MPTPs when setting $\beta_T = 5$ for optimized configurations obtained with (a) $l_C = 0.5L$; and (b) $l_C = L$.
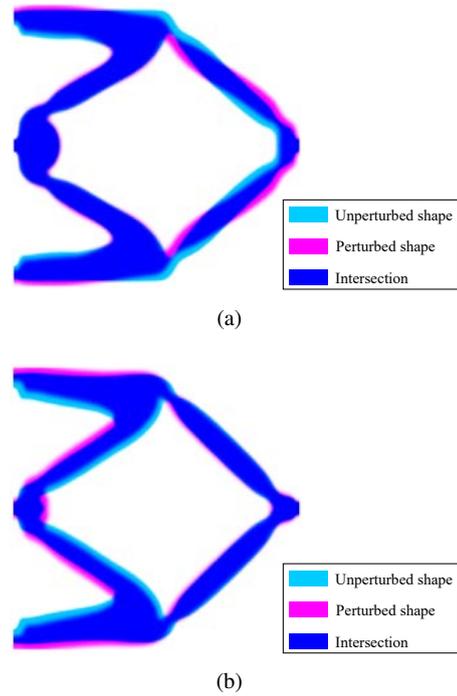

Fig. 17 Overlay image highlighting differences between unperturbed and perturbed shapes for optimized configurations obtained by $l_C = 0.5L$ and L.

for $l_C = 0.5L$ (Fig. 15(a)) and $l_C = L$ (Fig. 15(b)) have the same topology, but it is different from that for $l_C = 0.1L$ (Fig. 13(d)). The optimized configurations when $l_C = 0.5L$, and L have fewer linear elements than when $l_C = 0.1L$, and are similar to the deterministic solution, which again implies that geometrical uncertainty should be considered more when l_C is small.

Table 5 lists mutual mean compliance values calculated after optimization at the MPTPs of $\beta_T = 5$, with analysis settings of $l_C = 0.1L, 0.5L$, and L for each optimized configuration obtained for optimization settings of $l_C = 0.1L, 0.5L$, and L, respectively. This data indicates that diagonal compo-

nents are higher than or equal to the other components in the same row, as is the same in all previous tables. This demonstrates that the proposed method effectively considers the effect of l_C settings on the solutions.

Figure 16 shows the perturbed shapes at MPTPs for optimized configurations obtained with $l_C = 0.5L$ and L (Fig.15). Figure 17 highlights the differences between unperturbed (Fig. 15) and perturbed shapes (Fig. 16) for $l_C = 0.5L$ and L. Different from the case when $l_C = 0.1L$, linear elements change in their position and angle rather than their thickness when $l_C = 0.5L$ and L, which reflects the larger width of the autocorrelation function. Thus, we confirmed again that parameter l_C values have a significant effect on considered perturbation and obtained solutions, and therefore should be carefully set, depending on a particular manufacturing situation or usage environment.

7 Conclusion

This paper proposed a new reliability-based topology optimization method that operates under geometrical uncertainty. We achieved the following:

(1) Geometrical variations were modeled with an advection equation in which stochastic velocity was expressed using the K-L expansion. Based on this model, we formulated reliability-based topology optimization problems with a performance measure approach for inverse reliability.

(2) Based on the optimization formulations, we constructed an iterative two-level optimization algorithm that uses an inner iteration to search for MPTPs and an outer iteration that updates the design variables. In both optimization levels, sensitivities were systematically derived using the adjoint variable method.

(3) The proposed method was applied to two numerical examples to confirm its validity and utility. In the minimum mean compliance problem, we examined the dependencies of the optimal configurations on parameters β_T and l_C and confirmed that the proposed method successfully obtains optimized configurations reflecting these parameter settings. With increasing values of β_T, additional linear elements appeared in the optimized configurations, alleviating the influence of the shape perturbation on the objective function. On the other hand, with increasing values of l_C, the increasing width of the autocorrelation function reflected a relatively uniform shape perturbation, resulting in uniformly thicker structures, which are similar to the deterministic solution. Consequently, it is important to consider the geometrical uncertainty in topology optimization particularly when the magnitude of the variations is large and the correlation length of the variations is small.

(4) In the mutual mean compliance problem, the proposed method also effectively obtains optimal configurations, with geometries that reflect parameter β_T settings. With increasing values of β_T, linear structural elements in the corresponding optimized configurations were thicker near the boundaries where displacement was fixed or traction was applied, and supporting elements appeared near the boundary where the displacement was fixed, providing improved reliability against shape uncertainties.

The authors hope to conduct future research to reduce the computational cost of the proposed method, incorporating a single-loop approach for extending our method to 3-D design problems and obtaining solutions in practical computational time.

References

Alban A, Darji HA, Imamura A, Nakayama MK (2017) Efficient Monte Carlo methods for estimating failure probabilities. Reliability Engineering & System Safety 165:376–394

Alexandersen J, Aage N, Andreasen CS, Sigmund O (2014) Topology optimisation for natural convection problems. International Journal for Numerical Methods in Fluids 76(10):699–721

Allaire G (2002) Shape optimization by the homogenization method. Springer

Bendsøe MP, Kikuchi N (1988) Generating optimal topologies in structural design using a homogenization method. Computer Methods in Applied Mechanics and Engineering 71(2):197–224

Bendsøe MP, Sigmund O (1999) Material interpolation schemes in topology optimization. Archive of Applied Mechanics 69(9-10):635–654

Betz W, Papaioannou I, Straub D (2014) Numerical methods for the discretization of random fields by means of the Karhunen–Loève expansion. Computer Methods in Applied Mechanics and Engineering 271:109 – 129

Bichon BJ, McFarland JM, Mahadevan S (2011) Efficient surrogate models for reliability analysis of systems with multiple failure modes. Reliability Engineering & System Safety 96(10):1386–1395

Bourdin B (2001) Filters in topology optimization. International Journal for Numerical Methods in Engineering 50(9):2143–2158

Chen S, Chen W (2011) A new level-set based approach to shape and topology optimization under geometric uncertainty. Structural and Multidisciplinary Optimization 44(1):1–18

Chen S, Chen W, Lee S (2010) Level set based robust shape and topology optimization under random field uncertainties. Structural and Multidisciplinary Optimization 41(4):507–524

Chen X, Hasselman TK, Neill DJ, et al (1997) Reliability based structural design optimization for practical applications. In: Proceedings of the 38th AIAA/ASME/ASCE/AHS/ASC structures, structural dynamics, and materials conference, pp 2724–2732

Ezzati G, Mammadov M, Kulkarni S (2015) A new reliability analysis method based on the conjugate gradient direction. Structural and Multidisciplinary Optimization 51(1):89–98

Furuta K, Izui K, Yaji K, Yamada T, Nishiwaki S (2017) Level set-based topology optimization for the design of a peltier effect thermoelectric actuator. Structural and Multidisciplinary Optimization 55(5):1671–1683

Guest JK, Igusa T (2008) Structural optimization under uncertain loads and nodal locations. Computer Methods in Applied Mechanics and Engineering 198(1):116–124

Guest JK, Prévost JH, Belytschko T (2004) Achieving minimum length scale in topology optimization using nodal design variables and projection functions. International Journal for Numerical Methods in Engineering 61(2):238–254

Guo X, Zhang W, Zhang L (2013) Robust structural topology optimization considering boundary uncertainties. Computer Methods in Applied Mechanics and Engineering 253:356–368

Iga A, Nishiwaki S, Izui K, Yoshimura M (2009) Topology optimization for thermal conductors with heat convection and conduction including design-dependent effects. International Journal of Heat and Mass Transfer 52:2721–2732

Ito M, Kim NH, Kogiso N (2018) Conservative reliability index for epistemic uncertainty in reliability-based design optimization. Structural and Multidisciplinary Optimization 57(5):1919–1935

Jansen M, Lombaert G, Diehl M, Lazarov BS, Sigmund O, Schevenels M (2013) Robust topology optimization accounting for misplacement of material. Structural and Multidisciplinary Optimization 47(3):317–333

Jansen M, Lombaert G, Schevenels M (2015) Robust topology optimization of structures with imperfect geometry based on geometric nonlinear analysis. Computer Methods in Applied Mechanics and Engineering 285:452–467

Kang Z, Liu P (2018) Reliability-based topology optimization against geometric imperfections with random threshold model. International Journal for Numerical Methods in Engineering DOI 10.1002/nme.5797

Kawamoto A, Matsumori T, Yamasaki S, Nomura T, Kondoh T, Nishiwaki S (2011) Heaviside projection based topology optimization by a PDE-filtered scalar function.

Structural and Multidisciplinary Optimization 44(1):19–24

Keshtegar B, Lee I (2016) Relaxed performance measure approach for reliability-based design optimization. Structural and Multidisciplinary Optimization 54(6):1439–1454

Kharmanda G, Olhoff N, Mohamed A, Lemaire M (2004) Reliability-based topology optimization. Structural and Multidisciplinary Optimization 26(5):295–307

Kiureghian AD, Stefano MD (1991) Efficient algorithm for second-order reliability analysis. Journal of engineering mechanics 117(12):2904–2923

Kogiso N, Ahn W, Nishiwaki S, Izui K, Yoshimura M (2008) Robust topology optimization for compliant mechanisms considering uncertainty of applied loads. Journal of Advanced Mechanical Design, Systems, and Manufacturing 2(1):96–107

Kogiso N, Yang YS, Kim BJ, Lee JO (2012) Modified single-loop-single-vector method for efficient reliability-based design optimization. Journal of Advanced Mechanical Design, Systems, and Manufacturing 6(7):1206–1221

Lang C, Sharma A, Doostan A, Maute K (2015) Heaviside enriched extended stochastic FEM for problems with uncertain material interfaces. Computational Mechanics 56(5):753–767

Lazarov BS, Sigmund O (2009) Sensitivity filters in topology optimisation as a solution to Helmholtz type differential equation. In: 8th world congress on structural and multidisciplinary optimization

Lazarov BS, Schevenels M, Sigmund O (2012) Topology optimization with geometric uncertainties by perturbation techniques. International Journal for Numerical Methods in Engineering 90(11):1321–1336

Lee JO, Yang YS, Ruy WS (2002) A comparative study on reliability-index and target-performance-based probabilistic structural design optimization. Computers & structures 80(3):257–269

Ma ZD, Kikuchi N, Cheng HC (1995) Topological design for vibrating structures. Computer Methods in Applied Mechanics and Engineering 121(1):259–280

Matsumori T, Kondoh T, Kawamoto A, Nomura T (2013) Topology optimization for fluid–thermal interaction problems under constant input power. Structural and Multidisciplinary Optimization 47(4):571–581

Meng Z, Li G, Wang BP, Hao P (2015) A hybrid chaos control approach of the performance measure functions for reliability-based design optimization. Computers & Structures 146:32–43

Nishiwaki S, Frecker MI, Min S, Kikuchi N (1998) Topology optimization of compliant mechanisms using the homogenization method. International Journal for Numerical Methods in Engineering 42:535–559

Nouy A, Clement A (2010) eXtended Stochastic Finite Element Method for the numerical simulation of heterogeneous materials with random material interfaces. International Journal for Numerical Methods in Engineering 83(10):1312–1344

Rackwitz R, Flessler B (1978) Structural reliability under combined random load sequences. Computers & Structures 9(5):489–494

Rashki M, Miri M, Moghaddam MA (2014) A simulation-based method for reliability based design optimization problems with highly nonlinear constraints. Automation in Construction 47:24–36

Schevenels M, Lazarov BS, Sigmund O (2011) Robust topology optimization accounting for spatially varying manufacturing errors. Computer Methods in Applied Mechanics and Engineering 200(49):3613–3627

Sigmund O (2007) Morphology-based black and white filters for topology optimization. Structural and Multidisciplinary Optimization 33(4-5):401–424

Sigmund O (2009) Manufacturing tolerant topology optimization. Acta Mechanica Sinica 25(2):227–239

Sigmund O, Petersson J (1998) Numerical instabilities in topology optimization: a survey on procedures dealing with checkerboards, mesh-dependencies and local minima. Structural Optimization 16(1):68–75

Svanberg K (1987) The method of moving asymptotes–a new method for structural optimization. International Journal for Numerical Methods in Engineering 24(2):359–373

Tu J, Choi KK, Park YH (1999) A new study on reliability-based design optimization. Transactions-American Society of Mechanical Engineers Journal of Mechanical Design 121(4):557–564

Wang MY, Wang X (2004) "Color" level sets: a multi-phase method for structural topology optimization with multiple materials. Computer Methods in Applied Mechanics and Engineering 193(6):469–496

Xiao NC, Zuo MJ, Zhou C (2018) A new adaptive sequential sampling method to construct surrogate models for efficient reliability analysis. Reliability Engineering & System Safety 169:330–338

Yamada T, Izui K, Nishiwaki S (2011) A level set-based topology optimization method for maximizing thermal diffusivity in problems including design-dependent effects. Journal of Mechanical Design 133(3):031,011

Yin L, Ananthasuresh G (2001) Topology optimization of compliant mechanisms with multiple materials using a peak function material interpolation scheme. Structural and Multidisciplinary Optimization 23(1):49–62

Youn BD, Choi KK (2004) An investigation of nonlinearity of reliability-based design optimization approaches. Journal of Mechanical Design 126:403–411

Youn BD, Choi KK, Park YH (2003) Hybrid analysis method for reliability-based design optimization. Journal of Mechanical Design 125(2):221–232

Zhang W, Kang Z (2017) Robust shape and topology optimization considering geometric uncertainties with stochastic level set perturbation. International Journal for Numerical Methods in Engineering 110(1):31–56

Zuo W, Saitou K (2017) Multi-material topology optimization using ordered SIMP interpolation. Structural and Multidisciplinary Optimization 55(2):477–491